

# Calibration of colloid probe cantilevers using the dynamic viscous response of a confined liquid

Shannon M. Notley<sup>a)</sup> and Simon Biggs

*Centre for Multiphase Processes, The University of Newcastle, Callaghan, NSW 2308, Australia*

Vincent S. J. Craig<sup>b)</sup>

*Department of Applied Mathematics, Research School of Physical Sciences and Engineering, Australian National University, Canberra, ACT 0200, Australia*

(Received 6 August 2002; accepted 3 June 2003)

A method is described to determine the spring constant of colloid probe cantilevers used in force measurements with the atomic force microscope. An oscillatory drive applied to the substrate is coupled by viscous interactions to the colloid probe. The dynamic response of the probe, which is unaffected by static interactions, is then used to determine the spring constant of the cantilever. Thus an accurate calibration of the spring constant may be performed simultaneously with a normal colloidal probe force measurement *in situ*. © 2003 American Institute of Physics.

[DOI: 10.1063/1.1597950]

## I. INTRODUCTION

The atomic force microscope (AFM) is routinely used to measure a number of interfacial phenomena including surface forces,<sup>1-4</sup> friction,<sup>5-7</sup> and adhesion.<sup>8,9</sup> Of fundamental importance to these quantitative measurements is an accurate knowledge of the cantilever spring constant. Furthermore, by controlling the interaction geometry, it is possible to compare the measured interaction force with theory. Control of the interaction geometry and chemistry is often achieved by attaching a spherical colloid particle to the end of the cantilever.<sup>1,10,11</sup>

The spring constant is dependent upon the cantilever dimensions and material properties. Microfabricated cantilevers from the same batch or wafer often have uniform dimensions, but between batches, large variations in the spring constant of the same type of cantilever can occur. Insufficient control over the thickness of the cantilever is the greatest problem. The spring constant is proportional to the cube of the thickness, so small variations in thickness give rise to significant changes in the spring constant. These nonuniformities in the manufacturing process require that a measurement of the spring constant of each cantilever is essential for accurate, reproducible force measurements.

A variety of methods have been proposed to determine the cantilever spring constant.<sup>12-19</sup> Most are suited to cantilevers in the absence of an attached colloid particle. Indeed, no existing calibration technique can be used for all cantilever and interaction geometries. The two most commonly employed methods, the thermal noise method<sup>13</sup> and the added mass method,<sup>12</sup> determine the spring constant for a point load at the end of the cantilever. The spring constant can then

be corrected for the positioning of the colloidal particle away from the end of the cantilever.<sup>15</sup> The requirement to perform a correction increases the systematic error in the calibrated spring constant and fails to account for the altered compliancy of the cantilever due to the attachment of the particle with glue.

Recently a number of authors have proposed methods of calibrating AFM cantilever spring constants involving the hydrodynamic drag of the cantilever or a particle attached to a cantilever.<sup>18,19</sup> In the method of Maeda and Senden<sup>18</sup> a semiempirical relationship between the distributed load due to hydrodynamic drag on the cantilever and its static end loading is used to determine the spring constant. This method is unsuitable for colloid probes as the flow characteristics in the presence of an attached particle will differ greatly to that of a bare cantilever.

Craig and Neto<sup>19</sup> have used a force balance approach between the restoring force of the cantilever and the hydrodynamic drag force on a spherical particle approaching a wall. This method requires an accurate knowledge of the particle radius and solution viscosity. The deflection of the cantilever due to the hydrodynamic drag force is measured as a function of surface separation. In order to gain deflections of the cantilever that are both much greater than the static interaction force and measurable over a significant separation range, viscous fluids (viscosity  $\gg$  water) such as concentrated sucrose solutions and comparatively large surface approach velocities (ramp rates) are required. The asymptotic behavior of the hydrodynamic force at small separations introduces difficulties in the determination of the compliance region (required to calibrate optical sensitivity). Furthermore, the possibility of boundary slip complicates the analysis. This method provides an *in situ*, nondestructive measurement of the cantilever spring constant for the specific point of loading of the attached particle. However, in this method it is assumed that the deflection of the cantilever due to background surface forces is negligible.

<sup>a)</sup> Author to whom correspondence should be addressed; present address: Department of Fibre and Polymer Technology, Division of Fibre Technology, Royal Institute of Technology, Stockholm, Sweden; electronic mail: shannon@kth.se

<sup>b)</sup> Electronic mail: vince.craig@anu.edu.au

Here, a spring constant calibration method is described that uses the viscous response of a colloidal particle attached to a cantilever due to the normal oscillatory motion of a flat plane in a fluid medium. A small amplitude, high frequency sinusoidal wave form is superimposed on the normal ramp signal applied to the piezo. The dynamic deflection due to the hydrodynamic force and the static deflection due to surface forces are measured concurrently and evaluated independently.

Brenner<sup>20</sup> has given the exact expression for the hydrodynamic drag force on a sphere approaching a wall for low Reynolds number flow ( $<1$ ). It has been shown that when the distance between the sphere and wall is small in comparison to the radius of the sphere, the hydrodynamic drag force is given by Eq. (1), where  $\eta$  is the viscosity of the fluid,  $R$  is the radius of the particle,  $U$  is the velocity of approach, and  $D$  is the surface separation<sup>21,22</sup>

$$F_H = \frac{6\pi\eta R^2 U}{D}. \quad (1)$$

As the interaction geometry in our experimental arrangement is analogous to that in the surface forces apparatus (SFA), we can use the equations of motion derived by Israelachvili for the measurement of the viscosity of liquids in thin films.<sup>23</sup> The oscillatory response of the colloid probe due to the sinusoidal motion of the flat surface is measured as a function of mean surface separation. Assuming a no-slip boundary condition and that the liquid is Newtonian, the viscosity of liquid is given by Eq. (2), where  $\eta$  is the solution viscosity,  $k$  is the spring constant,  $D$  is the mean surface separation,  $R$  is the particle radius,  $\nu$  is the frequency of oscillation,  $A_0$  is the drive amplitude, and  $A$  is the amplitude of the gap separation. In the SFA,  $A$  is measured directly. In the AFM,  $A$  can be determined from measuring the amplitude response  $x_0$  and phase difference  $\theta$  between the drive and measured oscillatory signals and is given by Eq. (3)

$$\eta = \frac{kD}{12\pi^2 R^2 \nu} \left[ \left( \frac{A_0}{A} \right)^2 - 1 \right]^{1/2}, \quad (2)$$

$$A = |A_0 - x_0 e^{i\theta}|. \quad (3)$$

For a liquid of known viscosity and for a known particle radius the spring constant may be determined using Eq. (2). Alternatively, once the spring constant is accurately determined, the viscosity of small volumes of liquids in thin films can be measured. Equation (2) only holds for low inertial systems, that is when the driving frequency,  $\nu$ , is much less than the resonance frequency of the spring,  $\nu_0$ .

## II. EXPERIMENTAL METHODS

A number of modifications to the standard AFM force experiment were performed in order to simultaneously measure both static and dynamic forces between the substrate and colloid probe. Figure 1 shows a schematic representation of the experimental arrangement. The high voltage  $z$  ramp from the Nanoscope® controller, accessed via the signal access module (SAM) (Digital Instruments, CA), was coupled to a high frequency, small amplitude oscillatory signal pro-

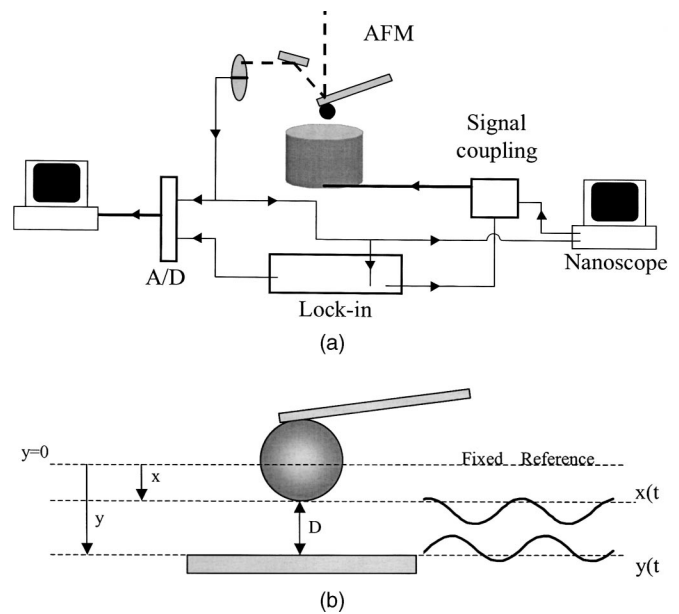


FIG. 1. (a) Flow diagram showing the connections to and from the AFM for the measurement of dynamic surface forces. (b) Schematic of the experimental arrangement for the measurement of hydrodynamic lubrication forces. The bottom surface oscillates at frequency  $\nu$  and driving amplitude  $A_0$ . Hydrodynamic forces cause the upper surface (colloid probe) to oscillate at the same frequency, however, the amplitude is attenuated and phase shifted by an amount  $\theta$ .

vided by a dual phase lock-in amplifier (SR 830, Stanford Research Systems). A summing audio transformer (Farnell A262A2E) was used to couple the signals. The coupled signal was then connected to the high voltage  $z$  input on the Nanoscope® SAM.

The hydrodynamic interaction couples the oscillatory motion of the flat surface to the colloid probe. The deflection of the cantilever due to the induced oscillatory motion of the colloid probe was measured by the split photodiode of the AFM. The dynamic response of the cantilever is the component of the response with the same frequency as the oscillatory signal. The output from the split photodiode was passed back to the lock-in amplifier where both the in phase and  $90^\circ$  out of phase components of the oscillatory signal were measured. These signals were used to determine the amplitude attenuation and phase difference between the motions of the substrate and colloid probe as a function of surface separation.

The output from the lock-in amplifier was measured using a 16-bit, analog-to-digital (A/D) converter capable of sampling at 100 kHz. This sampling rate is far greater than required and in these experiments the data were typically sampled at 2–5 kHz. The split photodiode output and signal applied to the  $z$  ramp were also sampled using this A/D converter. The digitized signals were then passed to a dedicated computer for processing. A customized program written in a commercial software package, Labview®, was used for data sampling and processing.

The static deflection of the cantilever due to surface forces was measured simultaneously with the oscillatory deflection due to hydrodynamic interactions. Zero surface separation ( $D=0$ ) was defined as the onset of the compliance

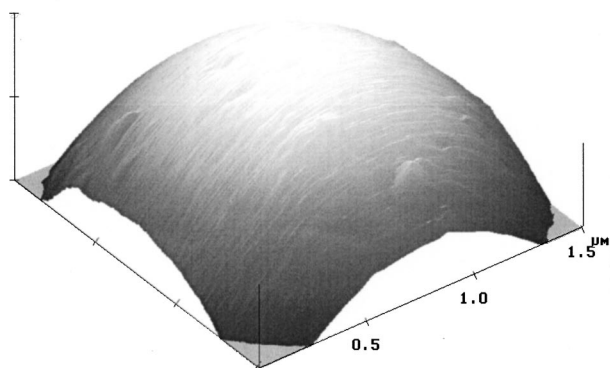


FIG. 2. AFM reverse image of the colloid probe obtained using the TGT-01 grating (NT-MDT, Russia). The presence of small surface asperities can be observed. Scan size is  $1.5 \times 1.5 \mu\text{m}^2$ , vertical axis is 25 nm/division.

region in the raw output of the static deflection versus piezo extension. The  $z$  ramp scan rate from the Nanoscope controller was typically set at approach velocities of less than 400 nm/s. Low ramp rates are employed ensuring that the static component of the interaction is attributable to surface forces and not to hydrodynamic interactions.

Typically, drive amplitudes of between 2 and 10 nm and frequencies less than 1000 Hz were used. Smaller drive amplitudes did not produce significant deflection of the cantilever at large surface separations. Furthermore, these frequencies were much less than the resonance frequency of the end loaded cantilever in aqueous solution (5–10 kHz) so inertial and acceleration terms can be ignored.

A smooth sphere was attached to an AFM cantilever using the method of Ducker *et al.*<sup>11</sup> Standard, V-shaped silicon nitride cantilevers (Digital Instruments, Santa Barbara, CA) were used in this study. Borosilicate glass spheres (Duke Scientific) with an approximate radius of 10  $\mu\text{m}$  (surface roughness  $< 0.15 \text{ nm rms}$  over  $100 \times 100 \text{ nm}^2$ ) were attached to the cantilever with a small amount of epoxy adhesive (Araldite, Selleys Co., Australia). A reverse imaging technique was used prior to the experiment to ensure that the colloidal probe was free of particulate debris.<sup>24</sup> Reverse imaging involves scanning the probe across an array of spikes with radius of curvature much less than that of the probe. A silicon grating (TGT-01, NT-MDT, Russia) was used in this case. An example image of the area of interaction of the colloid probe is shown in Fig. 2. The radius of the colloid probe was measured (to an accuracy of 0.1  $\mu\text{m}$ ) by scanning electron microscopy after the measurements. Freshly cleaved muscovite mica was used as the flat substrate. This substrate is atomically smooth and requires no further cleaning before use.

The AFM was housed in a temperature-controlled incubator. All measurements were performed at a constant temperature of  $20 \pm 0.1 \text{ }^\circ\text{C}$ . Water was used as a viscosity standard in order to determine the spring constant of the cantilever. Then the viscosity of several sucrose solutions was measured in order to validate the method. Aqueous solutions of  $\text{KNO}_3$  under a variety of  $p\text{H}$  conditions were used to alter the magnitude of the static interaction forces and thereby any possible effect on the dynamic component of the

interaction could be investigated. The solution  $p\text{H}$  was adjusted using an appropriate amount of aqueous  $\text{HNO}_3$  or  $\text{KOH}$ . All water used was purified using a Milli-Q purification unit. Sucrose (BDH)  $\text{KOH}$ ,  $\text{HNO}_3$ , and  $\text{KNO}_3$  (Sigma-Aldrich) were of AR grade. The  $\text{KNO}_3$  was baked at  $400 \text{ }^\circ\text{C}$  for 2 h before use.

The polymer used in this study was the weak cationic polyelectrolyte poly(2-vinylpyridine). Two samples of P2VP were obtained from Polysciences Inc. (Warrington, PA) and used without further purification. These samples were a relatively monodisperse P2VP with a molecular weight of 30 kDa ( $M_w/M_n \sim 1.27$ ) and a higher molecular weight, poly-disperse sample of 300–400 kDa.

The P2VP solutions were prepared by dissolving a known amount of polymer in an aqueous solution of  $\text{HNO}_3$ . The P2VP solution was gently stirred overnight at  $35 \text{ }^\circ\text{C}$  before being diluted as required with Milli-Q water. The  $p\text{H}$  of the P2VP solution was adjusted to 3.2 by the addition of an appropriate amount of  $\text{KOH}$  or  $\text{HNO}_3$  and the solution allowed to equilibrate for at least 24 h before being used in experimentation.

### III. RESULTS

The measured amplitude of the colloid probe due to the motion of the flat substrate in a typical experiment is shown in Fig. 3(a). The phase difference between the sinusoidal motions of the substrate and probe is also shown in Fig. 3(a). At large surface separations, the phase difference is close to  $90^\circ$  as would be expected for a purely viscous dissipation of energy. As the surfaces approach, the phase difference decreases and this corresponds with an increase in the measured amplitude of the colloid probe response due to increases in the hydrodynamic interaction. At a surface separation of 300 nm the measured amplitude of the colloid probe has increased significantly and the phase difference has decreased to  $70^\circ$ . As the surfaces approach the phase continues to decrease as the amplitude of response increases. At a surface separation of less than 20 nm the Van der Waals attractive force between the surfaces exceeds the spring restoring force and the two surfaces jump into contact. The phase difference decreases rapidly to  $0^\circ$  implying that the two surfaces are now moving in concert. This corresponds to the onset of the compliance region. The amplitude of the surface separation [calculated from Eq. (3)] is also presented in Fig. 3(a). At large surface separations, no deflection of the probe is measured so the gap amplitude is simply the drive amplitude. As the surfaces approach the gap amplitude decreases until at separations less than 25 nm, where the two surfaces are moving together, the gap amplitude tends to zero. Figure 3(b) shows the simultaneously recorded static force profile. The force-distance data is well fitted to DLVO theory in the limits of constant charge and constant potential and furthermore is consistent with previously published studies.<sup>4,25</sup> This shows that the surfaces are clean and fully wetting.

By rearranging Eq. (2), the spring constant of the cantilever can be determined from the slope of a plot of  $\beta$  [Eq. (4)] as a function of surface separation. Figure 4 shows such

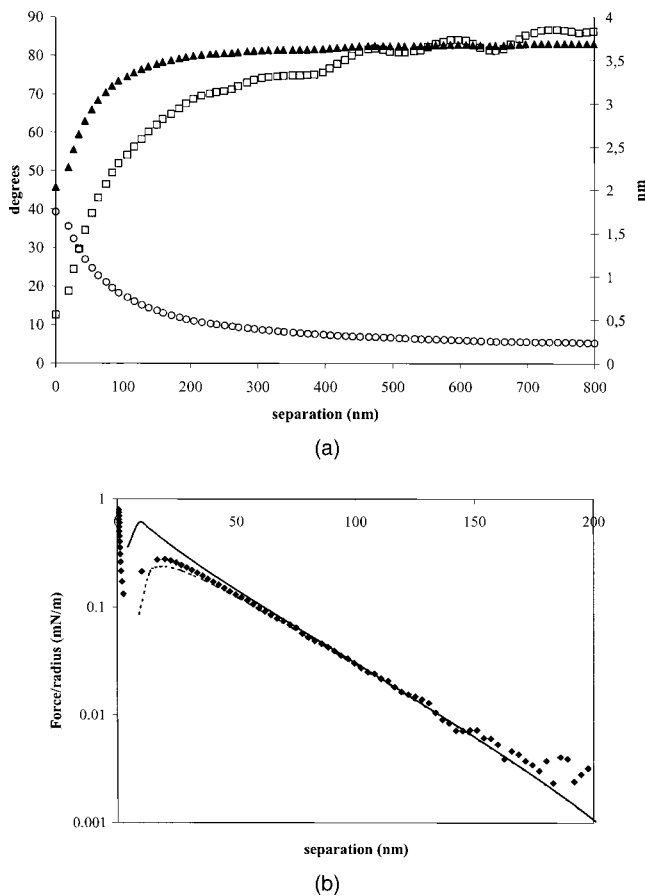


FIG. 3. (a) The measured amplitude of oscillation of the colloid probe (open circles) and phase difference between the oscillatory motion of the substrate and probe (open squares) as a function of surface separation in water (unadjusted pH, viscosity 1.000 mPa s). The static scan size was 1 μm and scan rate was 0.5 Hz. The oscillatory drive amplitude  $A_0$  was 3.7 nm and frequency 1000 Hz. The amplitude of surface separation (triangles) was determined from Eq. (3). Only every tenth measured point is shown for clarity. (b) Static surface forces upon approach of a 10.0 μm radius borosilicate sphere to a mica substrate in water. The best fit to DLVO for the surfaces in water (unadjusted pH) calculated from the nonlinear Poisson–Boltzmann equation in the limits of constant charge (solid line) and constant potential (dashed line) are also shown. The dissimilar fitting parameters were  $\psi_{\text{mica}} = 75$  mV,  $\psi_{\text{silica}} = 45$  mV,  $\kappa^{-1} = 32$  nm, and a Hamaker constant of  $1 \times 10^{-19}$  J. The scan size was 400 nm and scan rate was 0.5 Hz.

a plot used to determine the spring constant for a  $10.0 \pm 0.1$  μm radius silica particle attached to a 100 μm long, thick-legged Si<sub>3</sub>N<sub>4</sub> “V” shaped cantilever in water.

$$\beta = 12\pi^2 R^2 \eta \nu \left[ \left( \frac{A_0}{A} \right)^2 - 1 \right]^{-1/2} = kD. \quad (4)$$

A linear relationship is observed in Fig. 4 for surface separations between 25 and 300 nm. Instabilities of the colloid probe at surface separations of less than 20 nm due to Van der Waals forces cause the surfaces to rapidly jump into contact. Data in this region were not used in the spring constant calibration due to the instability of the cantilever. At surface separations greater than 300 nm the hydrodynamic coupling between the surface and the probe is small and the data is therefore dominated by noise. Hence data at separations greater than 300 nm were also excluded. The spring constant

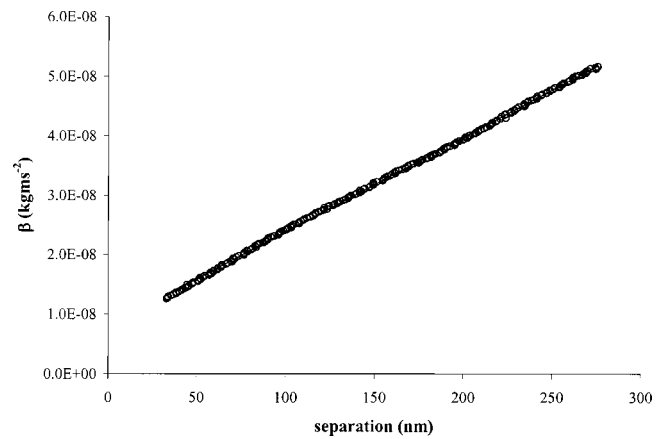


FIG. 4. Plot of  $\beta$  as a function of mean surface separation,  $D$ , for the interaction between a silica colloid probe (radius  $10.0 \pm 0.1$  μm) and mica substrate. The cantilever and surface are immersed in water (unadjusted pH, viscosity 1.000 mPa s). The static scan size was 1 μm and scan rate was 0.5 Hz. The oscillatory drive amplitude  $A_0$  was 3.7 nm and frequency 1000 Hz. From the linear regression ( $R^2$  is 0.9988), the measured spring constant was determined to be  $0.159 \pm 0.004$  N/m. The errors in the measurement are approximately the size of the data points along the vertical axis and significantly less along the distance axis.

was measured from the slope of the linear regression of the data points in Fig. 4 to be  $0.159 \pm 0.004$  N/m.

Once the cantilever spring constant was accurately determined, the response of the probe to the oscillatory motion of the flat substrate was used to measure the viscosity of aqueous sucrose solutions. Previously, the SFA has been used to measure the viscosity of liquids in thin films.<sup>22,23,26,27</sup> The SFA results show that simple liquids remain Newtonian or “bulk-like” in confined films as thin as 25 Å. Assuming that the liquid is Newtonian, the viscosity,  $\eta$ , is given by Eq. (2). Rearrangement of Eq. (2) into the familiar SFA form [Eq. (5)] makes the subject the effective mobility,  $G$ . When plotted as a function of surface separation the slope is equal to the inverse of the viscosity of the intervening fluid.

$$G = \frac{12\pi^2 R^2 \nu}{k} \left[ \left( \frac{A_0}{A} \right)^2 - 1 \right]^{-1/2} = \frac{1}{\eta} D. \quad (5)$$

Figure 5 presents the effective mobility,  $G$ , as a function of surface separation for aqueous sucrose solutions of different concentration. As the concentration of sucrose is increased, the measured slope ( $\eta^{-1}$ ) decreases. Some long wavelength oscillation of the data is evident due to optical interference. The measured viscosities of the sucrose solutions from the least-squares fit to the data in Fig. 5 are in excellent agreement with literature values<sup>28</sup> as compared in Table I.

The data in Fig. 3 were collected in water (pH 5.9). At this pH both the mica substrate and borosilicate glass probe have a negative surface charge. At surface separations less than 150 nm there is a significant repulsive interaction force due to the overlap of the electrical double layers of the probe and substrate. Figure 6(a) shows the measured equilibrium surface forces between the probe and substrate in solutions of  $1 \times 10^{-4}$  M KNO<sub>3</sub> in the pH range of 3.5–7.7.

Both the dynamic and static interactions were captured simultaneously. The spring constant used to calibrate the

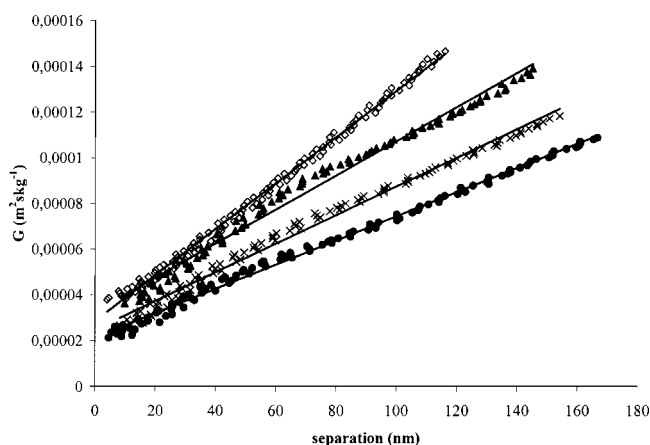


FIG. 5. Effective mobility is plotted vs separation. The slope of the plot is used to determine the viscosity of a range of aqueous sucrose solutions at 20 °C. A static scan size was 250 nm and scan rate was 0.5 Hz. An oscillatory drive amplitude of 3.7 nm and frequency of 200 Hz was used. The spring constant was  $0.070 \pm 0.003$  N/m and the particle radius was  $9.8 \pm 0.1$   $\mu$ m. The measured viscosity of the sucrose solutions is given in Table I. Water (open diamonds), 10% w/w sucrose/water (triangles), 15% w/w sucrose/water (crosses), and 20% w/w sucrose/water (circles).

static interaction was determined from the dynamic interactions as described above. Figure 6(b) shows  $\beta$  as a function of surface separation for each of the data sets shown in Fig. 6(a). Note that the data have been offset to allow ease of comparison between the gradients. The least-squares fit to the four curves agree to within 2%. The data in Fig. 6(b) show clearly that deflections of the cantilever due to static interaction forces do not affect the response of the cantilever due to the hydrodynamic interactions.

Limitations of the approach adopted here were investigated using measurements for similar probes carrying adsorbed polymer films. In the first example, a molecularly thin layer of polymer was deposited on each surface by free adsorption of a low molecular weight highly charged polyelectrolyte from a low concentration solution. Previous reports have concluded, from static force data, that the adsorbed film is at most 2 to 3 nm thick.<sup>29,30</sup> Such a surface has been postulated as a good model for a rough surface. In the second case, a high molecular weight sample of the same polymer was adsorbed from a high concentration solution. This is known to result in the development of a significant steric boundary layer. Previous drainage measurements on such systems have indicated that solvent will penetrate into this “soft” polymer layer. This surface may therefore be considered as a model for a soft deformable colloid probe. Typical

TABLE I. Comparison of the measured viscosity determined using Eq. (5) and the data presented in Fig. 4 to the bulk literature viscosity of aqueous sucrose solutions. Note that the data for water is used to determine the spring constant.

| Concentration (wt %) | Measured viscosity (mPa s) | Literature viscosity (mPa s) |
|----------------------|----------------------------|------------------------------|
| 0                    |                            | 1.00                         |
| 10                   | $1.34 \pm 0.03$            | 1.31                         |
| 15                   | $1.60 \pm 0.03$            | 1.59                         |
| 20                   | $1.89 \pm 0.04$            | 1.92                         |

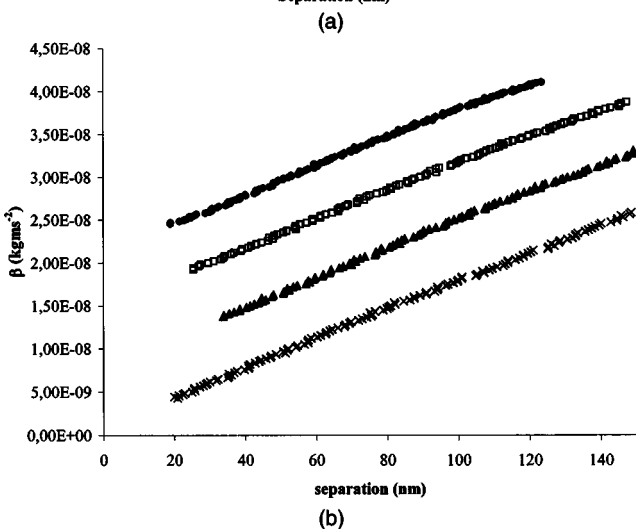
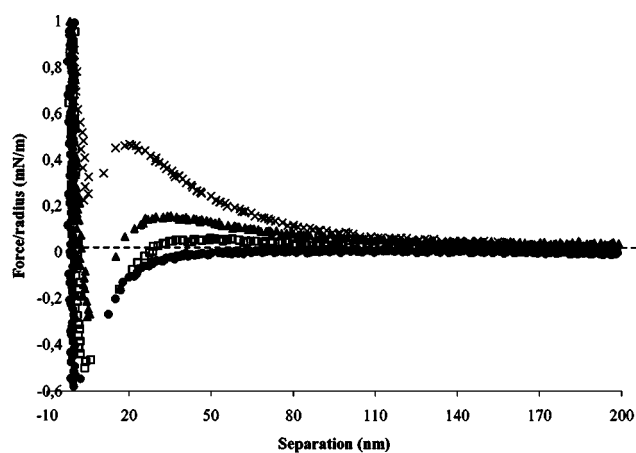


FIG. 6. (a) Equilibrium surface forces on approach between a mica substrate and borosilicate glass probe (radius  $10.0 \pm 0.1$   $\mu$ m) as a function of solution pH. The static scan size was 250 nm and scan rate was 0.5 Hz for all force experiments. The repulsive electrostatic component of the force increases with pH due to a corresponding increase in surface charge. pH 3.5, circles; 4.5, squares; 5.9, triangles; and 7.7, crosses. (b) A plot of  $\beta$  vs separation, used to determine the spring constant of the cantilever. The measured spring constants under different static deflection conditions, as measured from least-squares fits to the four data sets, agree to within 2%. The curves are offset for clarity. pH 3.5, circles; 4.5, squares; 5.9, triangles; and 7.7, crosses.

static force data for these two systems are shown in Fig. 7. Clearly, there is no evidence of a steric layer in the presence of the low molecular weight polymer. In contrast, the high molecular weight polymer sample shows a long range steric repulsion under the conditions of the experiment. Corresponding hydrodynamic data for these force curves are shown in Fig. 8. At large separations, all three data sets are linear and the gradient of the best fits to the data in these linear regions are equivalent suggesting that the surface character does not affect the measurement of  $k$ . Clearly, the data for the two polymer samples are not linear over the whole range of surface separation distances and the adsorbed film does influence the fluid drainage. The range of this deviation is related to the extension of the polymer layer away from the surface.

#### IV. DISCUSSION

The calibration of AFM cantilever spring constants using the viscous response of a confined liquid has a number of

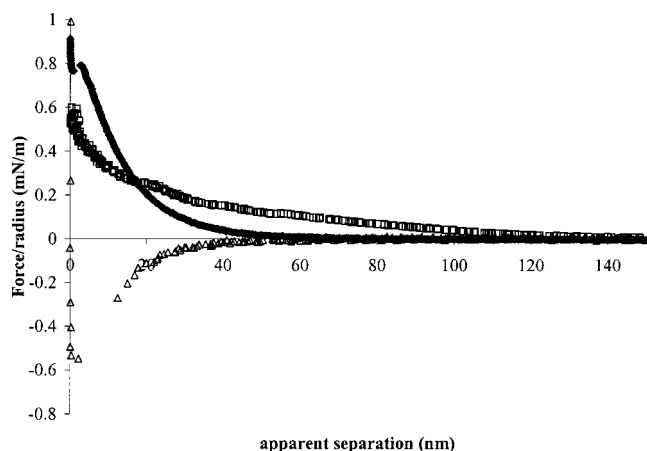


FIG. 7. Normalized static surface forces as a function of distance for bare (closed diamonds), low molecular weight P2VP (open squares), and high molecular weight P2VP covered surfaces (open triangles) at pH 3. A scan rate of 0.5 Hz and scan size of 300 nm was used for all experiments.

advantages over other methods. This method determines the spring constant with the probe attached and the effect on the spring constant of the placement of the probe is internally accounted for. Most existing methods determine the spring constant for a point load at the end tip of the cantilever. The spring constant is then corrected for distance of the probe from the end of the cantilever. This assumes that the cantilever has a uniform cross section and that the material properties of the cantilever are constant throughout the length of the beam. If the method requires a correction, the systematic error of the measurement of the spring constant is increased. Also other methods fail to adequately account for the possible altered compliancy of the cantilever when a colloidal particle is attached with glue. Using the proposed method a quick, *in situ* determination of the cantilever spring constant can be made. Indeed, the data required to determine the spring constant can be captured concurrently with the force data of interest. Although nonstandard electronics are required for the determination of the spring constant using this method, the necessary components are readily available and easily implemented into the experimental instrumentation.

Examination of Eq. (4) indicates that there are two contributing sources of error in the determination of absolute

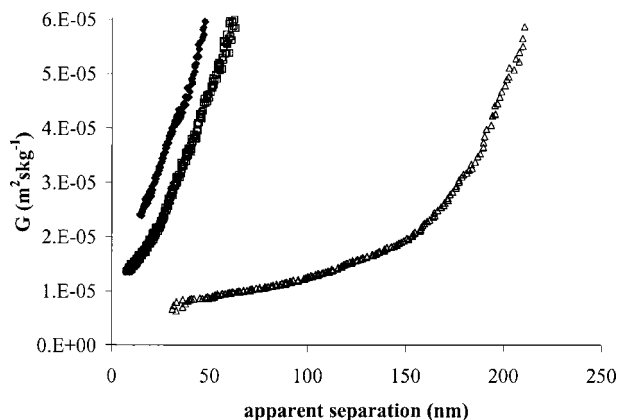


FIG. 8. Effective mobility as a function of separation for the system described in Fig. 7.

values for  $\beta$  and hence the spring constant determination, viz. the particle radius,  $R$ , and the surface separation distance,  $D$ . The precise control of temperature afforded by the incubation of the AFM ensures a highly precise viscosity for our solvent standard (water). Typically the radius of the particle in these experiments can be measured to an accuracy of  $\sim 1\%$  using scanning electron microscopy (SEM). Since in the determination of the spring constant the radius is squared in the calculation, this introduces an error of 2% in the measured value. Accurate knowledge of the separation distance relies upon precise calibration of the AFM drive piezo and an accurate definition of the zero distance. Both factors can introduce error into absolute values of  $\beta$ . However, it should be noted that to obtain the value of  $k$ , it is not necessary to know the absolute values of  $\beta$ , only the variation of  $\beta$  with distance. Hence there is no absolute requirement to know zero separation. Of course, the movement of the piezo must still be accurately known such that a value of  $\Delta D$  can be obtained. Typically, the movement of the piezo can be accurately calibrated with  $<0.1\%$  error. Hence this is not expected to be significant when compared to the error from the particle radius. Thus an accurate spring constant can be obtained at an arbitrary set of separation distances provided that the distance moved ( $\Delta D$ ) is accurately known and that the response of  $\beta$  with  $D$  is linear (Fig. 4). Obviously, the probe and surface should be close enough to ensure an amplitude response that is sufficiently greater than thermal noise. Also, the limitations of the hydrodynamic theory are such that the distance of surface separation is small compared to the particle radius. For a  $10\ \mu\text{m}$  radius bead, as used here, this typically limits us to separations of less than  $1\ \mu\text{m}$ . Other contributing sources of error in the measurement of the spring constant using this method need also to be considered. For example, typical errors in the calibration of the optical sensitivity may be of the order of 1% to 2%.

Optical noise can contribute to nonlinearity in the plots of beta versus separation. This can lead to significant variations in the slope (up to 10%) over subsets of the data. In order to minimize the error in the determined spring constant it is recommended that data be obtained over as large a distance range as practicable. When the nonlinearity due to optical noise is significant the error in the determined spring constant will be as large as 10%, which is comparable to other methods. Noncoherent light sources are now available that will remove this source of error allowing the technique to give spring constants with an accuracy of  $\sim 4\%$ .

The data in Figs. 7 and 8 indicate clearly that the nature of the surface is unimportant in the measurement of a spring constant using this approach, provided that the intervening solvent is Newtonian and that its viscosity is accurately known. Again, accurate calibration relies upon performing a measurement in the linear region of  $\beta$  versus  $D$ . Thus it appears that this calibration procedure will be applicable to a wide range of probe materials whether hard (as in this case of a silica particle interacting with a mica substrate) or soft (for example, surfaces with adsorbed species), rough or smooth.

No attempt has been made to systematically quantify the effects of surface roughness for the bare particles on the

measured spring constant. At small surface separations (of the order of the roughness) the lubrication force may be influenced by surface roughness. However, data at small surface separations were rejected in the spring constant determination due to the cantilever instability caused by Van der Waals attractive forces. Significant effects from surface roughness may be expected to cause deviations from the linear behavior, as seen for adsorbed polymer films. In principle, this calibration method can be used for a range of cantilever spring constants and probe sizes. The limiting factor is the hydrodynamic force required to cause a measurable oscillatory deflection of the cantilever. Thus this method is ideal for most standard contact cantilevers and colloid probe sizes of 5  $\mu\text{m}$  diameter or greater. However, this method would be unsuitable for the much stiffer, tapping mode cantilevers.

### ACKNOWLEDGMENTS

S.N. and S.B. acknowledge the support of the Center for Multiphase Processes, a Special Research Center of the Australian Research Council. V.C. acknowledges support from the Australian Research Council for the provision of a Postdoctoral Fellowship.

<sup>1</sup>W. A. Ducker, T. J. Senden, and R. M. Pashley, *Langmuir* **8**, 1831 (1992).

<sup>2</sup>I. Larson, C. J. Drummond, D. Y. C. Chan, and F. Grieser, *J. Am. Chem. Soc.* **115**, 11885 (1993).

<sup>3</sup>S. Biggs and P. Mulvaney, *J. Chem. Phys.* **100**, 8501 (1994).

<sup>4</sup>P. G. Hartley, I. Larson, and P. J. Scales, *Langmuir* **13**, 2207 (1997).

<sup>5</sup>R. W. Carpick and M. Salmeron, *Chem. Rev. (Washington, D.C.)* **97**, 1163 (1997).

<sup>6</sup>B. Bhushan, *Int. Mater. Rev.* **44**, 105 (1999).

<sup>7</sup>S. Biggs, R. Cain, and N. W. Page, *J. Colloid Interface Sci.* **232**, 133 (2000).

<sup>8</sup>M. Radmacher, J. P. Cleveland, M. Fritz, H. G. Hansma, and P. K. Hansma, *Biophys. J.* **66**, 2159 (1994).

<sup>9</sup>S. Biggs and G. Spinks, *J. Adhes. Sci. Technol.* **12**, 461 (1998).

<sup>10</sup>H.-J. Butt, *Biophys. J.* **60**, 1438 (1991).

<sup>11</sup>W. A. Ducker, T. J. Senden, and R. M. Pashley, *Nature (London)* **353**, 239 (1991).

<sup>12</sup>J. P. Cleveland, S. Manne, D. Bocek, and P. K. Hansma, *Rev. Sci. Instrum.* **64**, 403 (1993).

<sup>13</sup>J. L. Hutter and J. Bechhoefer, *Rev. Sci. Instrum.* **64**, 1868 (1993).

<sup>14</sup>T. J. Senden and W. A. Ducker, *Langmuir* **10**, 1003 (1994).

<sup>15</sup>J. E. Sader, I. Larson, P. Mulvaney, and L. R. White, *Rev. Sci. Instrum.* **66**, 3789 (1995).

<sup>16</sup>D. A. Walters, J. P. Cleveland, N. H. Thomson, P. K. Hansma, M. A. Wendman, G. Gurley, and V. Elings, *Rev. Sci. Instrum.* **67**, 3583 (1996).

<sup>17</sup>J. E. Sader, *J. Appl. Phys.* **84**, 64 (1998).

<sup>18</sup>N. Maeda and T. J. Senden, *Langmuir* **16**, 9282 (2000).

<sup>19</sup>V. S. J. Craig and C. Neto, *Langmuir* **17**, 6018 (2001).

<sup>20</sup>H. Brenner, *Chem. Eng. Sci.* **16**, 242 (1961).

<sup>21</sup>G. D. M. Mackay and S. G. Mason, *J. Colloid Sci.* **16**, 632 (1961).

<sup>22</sup>D. Y. C. Chan and R. G. Horn, *J. Chem. Phys.* **83**, 5311 (1985).

<sup>23</sup>J. N. Israelachvili, *J. Colloid Interface Sci.* **110**, 263 (1986).

<sup>24</sup>C. Neto and V. S. J. Craig, *Langmuir* **17**, 2097 (2001).

<sup>25</sup>G. Toikka and R. A. Hayes, *J. Colloid Interface Sci.* **191**, 102 (1997).

<sup>26</sup>J. Klein, Y. Kamiyama, H. Yoshizawa, J. N. Israelachvili, G. H. Fredrickson, P. Pincus, and L. J. Fetters, *Macromolecules* **26**, 5552 (1993).

<sup>27</sup>S. E. Campbell, G. Luengo, V. I. Srdanov, F. Wudl, and J. N. Israelachvili, *Nature (London)* **382**, 520 (1996).

<sup>28</sup>*CRC Handbook of Chemistry and Physics*, 77th ed. (CRC, Boca Raton, FL, 1996).

<sup>29</sup>J. Marra and M. L. Hair, *J. Phys. Chem.* **92**, 6044 (1988).

<sup>30</sup>S. Biggs and A. D. Proud, *Langmuir* **13**, 7202 (1997).